

X-611-68-353

PREPRINT

NASA TM X-63351

2-20 KEV SPECTRUM OF X-RAYS FROM THE CRAB NEBULA AND THE DIFFUSE BACKGROUND NEAR GALACTIC ANTICENTER

ELIHU A. BOLDT
UPENDRA D. DESAI
STEPHEN S. HOLT

GPO PRICE \$ _____

CSFTI PRICE(S) \$ _____

Hard copy (HC) _____

Microfiche (MF) _____

SEPTEMBER 1968

ff 653 July 65



GODDARD SPACE FLIGHT CENTER

GREENBELT, MARYLAND

N 68-35732 _____

(ACCESSION NUMBER)

(THRU)

26
(PAGES)

(CODE)

TMX-63351
(NASA CR OR TMX OR AD NUMBER)

(CATEGORY)

FACILITY FORM 602



X-611-68-353

PREPRINT

2-20 keV SPECTRUM OF X-RAYS FROM THE
CRAB NEBULA AND THE DIFFUSE BACKGROUND
NEAR GALACTIC ANTICENTER

Elihu A. Boldt, Upendra D. Desai
and Stephen S. Holt

September 1968

NASA/GODDARD SPACE FLIGHT CENTER
Greenbelt, Maryland

PRECEDING PAGE BLANK NOT FILMED.

2-20 keV SPECTRUM OF X-RAYS FROM THE
CRAB NEBULA AND THE DIFFUSE BACKGROUND
NEAR GALACTIC ANTICENTER

Elihu A. Boldt, Upendra D. Desai
and Stephen S. Holt

ABSTRACT

Data are presented from a rocket-borne exposure to x-rays from the Crab Nebula and its apparently source-free neighborhood on the celestial sphere near galactic anticenter. With ~ 2 keV resolution, the Crab Nebula is found to have a structureless spectrum which is consistent with a power law of index $-1.93 \pm .05$ in the differential photon flux between 2-20 keV, in substantial agreement with results of investigators using balloon-borne detectors at higher energies. The diffuse x-ray background is found to exhibit a harder spectrum than the Crab Nebula in the same energy range. The 2-20 keV background spectrum, with index $-1.3 \pm .1$, is significantly flatter than that reported at higher energies.

5

PRECEDING PAGE ~~BLANK~~ NOT FILMED.

CONTENTS

	<u>Page</u>
ABSTRACT	iii
INTRODUCTION	1
EXPERIMENTAL PROCEDURE	1
EXPERIMENTAL RESULTS	3
CRAB NEBULA	4
DIFFUSE X-RAY BACKGROUND	7
REFERENCES	9
APPENDIX—DATA RETRIEVAL	11

2-20 keV SPECTRUM OF X-RAYS FROM THE
CRAB NEBULA AND THE DIFFUSE BACKGROUND
NEAR GALACTIC ANTICENTER

Elihu A. Boldt, Upendra D. Desai
and Stephen S. Holt

September 1968

NASA/GODDARD SPACE FLIGHT CENTER
Greenbelt, Maryland

2-20 keV SPECTRUM OF X-RAYS FROM THE
CRAB NEBULA AND THE DIFFUSE BACKGROUND
NEAR GALACTIC ANTICENTER

I. INTRODUCTION

The Crab Nebula (Tau XR-1) was one of the first discrete x-ray sources to be discovered and the first to be correlated with an optical object (Bowyer, et al (1964)). While most of the experimental data have suggested a synchrotron model for the x-radiation from the Crab Nebula, Sartori and Morrison (1967) have pointed out that a superposition of thermal sources might adequately fit the observed emission. As described below, the presently reported data lend considerable support to the synchrotron hypothesis.

The presently reported background observation is a new contribution to the data library which lends strong confirmation to previous indications (Seward, et al (1967), Henry, et al (1968)) that the spectrum between 2 and 20 keV is flatter than the spectrum well above 20 keV, with an apparent change of spectral index of about unity over the two regions.

II. EXPERIMENTAL PROCEDURE

An (six-element) x-ray detector was carried aloft on an Aerobee 150 rocket from White Sands, N.M. at 20:15 MST on March 15, 1968. The detector consisted of three 6" x 2" x 2" argon-filled proportional counters with .002" beryllium windows in front of three krypton-filled proportional counters, all at a pressure of 1 atmosphere, as shown in Figure 1. The signals from all six counters were in mutual anti-coincidence, and in anti-coincidence with the signal of the plastic guard scintillator in which the counters were contained. A

multi-layer graded (Sn-Cu-Al) shield surrounded the plastic scintillator. Supplementary beam definition was supplied by two multi-layer (Al-Cu-Al) stationary plates used for collimation and a rotating multi-layer plate that intercepted the beam, modulating the acceptance aperture for detected x-rays. The rotating plate was driven by a stepping motor through 10 equally spaced dwell positions with a period of 27 sec for one complete rotation.

On ascent, the detector was completely contained within the rocket cylinder, and had Fe^{56} and Sn^{119} sources in its field of view for energy calibration. Prior to apogee, the side door of the vehicle was opened and the detector was deployed to a direction normal to the rocket axis. The orientation of the rocket was determined by an attitude control system (ACS) such that the detector was pointed at six fixed targets on the celestial sphere for durations of approximately 30 seconds each. The six fixed ACS targets and the associated detector fields of view on the celestial sphere are represented schematically in Figure 2. The precise coordinates of the ACS positions were determined by the use of a Nikon F camera which was aligned with the x-ray detector axis, and which took pictures of the star field at 8 second intervals (so that there were at least three exposures per ACS position). After the completion of the sixth ACS position, the detector was returned to the interior of the vehicle and recalibrated with the iron and tin sources during descent.

The six ACS positions were chosen such that positions #1 and #6 gave Crab-independent determinations of the background above and below the plane of the galaxy. The rotating plate, by changing the acceptance solid angle, could, in principle, provide the means for separating the true diffuse x-ray sky background from any apparent detector background induced by the radiation environment. In

ACS positions #2 and #5 the x-ray beam from the Crab Nebula is modulated for the central counters while in positions #3 and #4 this beam is modulated for the side counters. A comparison of Figure 1 and Figure 2 with the experimental data of Figure 3 should clarify the scheme of this observational program.

III. EXPERIMENTAL RESULTS

The presence of RF interference during the experiment generated a large dead time, so that only about 16% of the data was retrieved. That portion of the data which was used was clean, however, so that the experimentally observed spectrum should be correct (see Appendix for a full discussion of the data retrieval). There is some uncertainty beyond statistical in the normalization of the obtained spectra, but the precision in the determination of the spectral shape itself is limited only by the available statistics and resolution.

Figure 3 displays the observed raw counting rates of the three argon detectors during the experiment. The time interval used is 2.644 sec, which corresponds to the time spent in each fixed position of the rotating plate.

In order to determine the Crab Nebula spectrum, the counting rates in ACS positions #1 and #6 were used for a baseline. These counting rates represent the total background contamination of the Crab exposure (i.e. true diffuse x-ray background plus detector contamination). As explained in the Appendix, the percentage of the total incident photon flux which is recorded does not sensibly change as the incident photon flux changes. Therefore, this baseline may be subtracted directly from the Crab exposure, without any correction factor, in order to obtain the raw Crab counting rates. These net counting rates, corrected for counter efficiency, are displayed in Figure 4.

An unambiguous determination of the diffuse background is much more difficult to obtain. Had we not lost ~84% of the data, we would have been able to use a statistically significant modulation pattern in the counting rates in ACS positions #1 and #6 to determine the relative contributions of diffuse x-ray background and detector contamination. With the available statistics, however, we can only determine that the modulation is consistent with the ~30% expected. We have estimated the contribution of internal background to this spectrum by considering the background during ascent and descent in that counter which was completely occulted by the rotating plate (for one particular position of this plate) in viewing the calibration sources within the vehicle on ascent and descent. This contribution was about 10% of the observed counting rate, and was subtracted. Figure 5 displays the spectra observed in the three argon counters in ACS positions #1 and #6.

IV. CRAB NEBULA

From Figure 4, it is clear that a power law yields a good representation of the x-ray spectrum of the Crab Nebula between 2-20 keV. The best fit power law spectrum obtained from each of the three argon counters are presented in Table I. The absolute normalization of the spectrum obtained with counter II is indicated as being approximate. This is because the disposition of counter II directly below the rotating collimator made the determination of the absolute efficiency of this counter less reliable than that of counters I and III. Since the counters were nominally identical, we have used the mean efficiency of counters I and III for the approximate efficiency of counter II.

Table II summarizes the results of this measurement along with recent measurements of the spectrum of Tau XR-1 carried out by several investigators,

Table I

Best Fit to $AE^{-\alpha} \text{ cm}^{-2} \text{ sec}^{-1} \text{ keV}^{-1}$ for Tau XR-1 Between 2-20 keV

Counter	A	α
I	9.1	$1.97 \pm .09$
II	~ 8.7	$1.88 \pm .09$
III	7.9	$1.94 \pm .09$

$\left. \begin{array}{l} 1.97 \pm .09 \\ 1.88 \pm .09 \\ 1.94 \pm .09 \end{array} \right\} 1.93 \pm .05$

Table II

Spectral Measurements of Tau XR-1

Observations	Spectral Interval	Spectral Index (α)
1) Rocket-borne argon proportional counters; this experiment	2-20 keV	1.93 ± 0.05
2) Rocket-borne argon proportional counter; Grader et al 1966	1-10 keV	2.3 ± 0.2
3) Balloon-borne CsI(Tl) scintillator; Riegler et al 1968	20-70 keV	2.0 ± 0.3
4) Balloon-borne NaI(Tl) scintillator; Peterson et al 1968	20-200 keV	1.91 ± 0.1
5) Balloon-borne NaI(Tl) scintillator; Haymes et al 1968	40-500 keV	2.19 ± 0.08
6) Balloon-borne Ge(Li) crystal; Jacobson 1968	20-200 keV	2.13

using a variety of techniques. The individual spectral coverage provided by most of these experiments is a decade or more in photon energy. Due to uncertainties in the calibration of the absolute efficiency of detectors, the most reliable comparison among the observations is taken to be the measured spectral index (α) for the photon flux. The weighted mean (weighting factor = σ^{-2}) spectral index of the five measurements where errors (σ) are quoted is $\alpha = 2.00$; this is the best estimate of the spectral index over the 1-500 keV band. For measurements below 20 keV (observations #1 and #2, Table II), the weighted mean spectral index is $\alpha = 1.95$, while the weighted mean spectral index for measurements above 20 keV (observations #3, #4, #5) is $\alpha = 2.08$. A spectrum consistent with most observations 1-500 keV, is $\sim 7 E^{-2}$ photons/cm²-sec-keV, where E is the photon energy in keV. An extrapolation of this single power law spectrum to the optical continuum intercepts recent measurements by Ney and Stein (1968), at 3.5 microns. Therefore, a power law synchrotron model for the x-ray emission from the Crab Nebula is clearly indicated.

Although the synchrotron hypothesis provides a simple explanation of the x-ray spectral shape, Sartori and Morrison (1967) have pointed out that a superposition of thermal sources could also yield an approximation to the observed x-ray emission spectrum. In a recent study (Holt et al 1968) it has been shown that the expected iron line emission from such a thermal source should be evident. The presently reported data were used in that study to exhibit that there is no evidence for such line emission, at a statistical level exceeding 1σ for any relevant model of elemental abundances. Inspection of Figure 4 in the neighborhood of 7 keV shows no indication of iron emission.

V. DIFFUSE X-RAY BACKGROUND

The diffuse x-ray background may also be fitted by a power law. The best fits to the data of Figure 5 are given in Table III.

Table III
Best Fit to $AE^{-\alpha} \text{ cm}^{-2} \text{ sec}^{-1} \text{ keV}^{-1} \text{ sr}^{-1}$ for the Diffuse
X-ray Background Between 2-20 keV

Counter	A	α
I	5.7	$1.23 \pm .16$
II	~ 6.3	$1.25 \pm .18$
III	6.7	$1.37 \pm .18$

$\left. \begin{array}{l} 1.23 \pm .16 \\ 1.25 \pm .18 \\ 1.37 \pm .18 \end{array} \right\} 1.3 \pm .1$

The spectra have been evaluated after subtracting out the $\sim 10\%$ internal background as described above. It is worth noting that the shape of the background spectrum is not sensitive to this subtraction. It should be noted, as well, that there seem to be systematic prominences in the background spectra at energies corresponding to the K x-rays of argon and krypton (2.96 and 12.65 keV, respectively). This might be the result of dead regions and/or insufficiently low thresholds (the thresholds for each of the counters is $\sim .3$ keV), but it is difficult to understand why these prominences would not show up in the Crab spectrum as well. The Crab spectrum is steeper, so that the effect will be smaller if dead regions in the counters are responsible, but there is no hint of the effect in Figure 3. In any case, the best fit spectrum is not affected by these prominences. ACS positions #1 and #6 were used in the spectral determinations. Within statistics, we could not differentiate between the spectra for the fields of view above and

below the plane of the galaxy, or between them and the records we have in ACS positions #2-#5 where one of the counters has its response to the Crab completely occulted during the modulation by the rotating plate.

The spectrum we measure is consistent with the assumption that the background spectrum steepens with increasing energy. Results between 20-200 keV from balloon-borne platforms (c.f. Bleeker, et al (1968)) yield a spectral index of -2.4 ± 0.2 , while the results of Seward, et al (1967) yield an index of -1.6 between 4-40 keV. In a recent rocket exposure, Henry, et al (1968) have found an index of $-1.4 \pm .1$ in the energy range 1.5-8 keV. The latter investigators have attributed the observed spectral break in the spectrum at ~ 10 keV to an intrinsic break at ~ 1.5 BeV in the spectrum of electrons generating inverse Compton x-rays according to the model proposed by Felten and Morrison (1966). Our confirmation of the hard spectrum below 10 keV supports the conclusion that there is a change in the background x-ray spectral index of about unity over the region ~ 10 -20 keV.

It is a pleasure to thank Messrs F. Birsa, R. Bleach, A. Booth, C. Cancro, R. Pincus, R. Tatum, and M. Ziegler for their particularly important technical contributions and Drs. E. Roelof and P. Serlemitsos for valuable discussions.

REFERENCES

- Bleeker, J. A. M., Burger, J. J., Deerenberg, A. J. M., Scheepmaker, A.,
Swanenburg, B. N. and Tanaka, Y., Hayakawa, S., Makino, F., and Ogawa,
H., 1968, Canadian Journal of Physics 46, S461.
- Boyer, C. S., Byram, E. T., Chubb, T. A., and Friedman, H., 1964, Science 146,
912.
- Cancro, C., Crockett, W., Garrahan, N., and McGowan, R., 1968, NASA-Goddard
Document X-711-68-74 (to be published).
- Felten, J. E., and Morrison, P., 1966, Ap. J. 146, 686.
- Grader, R. J., Hill, R. W., Seward, F. D., and Toor, A., 1966, Science 152, 1499.
- Haymes, R. C., Ellis, D. V., Fishman, G. J., Kurfess, J. D. and Tucker, W. H.,
1968, Ap. J. 151, L9.
- Henry, R. C., Fritz, G., Meekins, J. F., Friedman, H., and Byram, E. T., 1968,
Ap. J. 153, L11.
- Holt, S. S., Boldt, E. A., and Serlemitsos, P. J., 1968, Ap. J. (submitted).
- Jacobson, A. S., 1968, Ph.D. dissertation, University of California, San Diego
SP-68-2.
- Ney, E. P., and Stein, W. A., 1968, Ap. J. 152, L21.
- Peterson, L. E., Jacobson, A. S., Pelling, R. M., Schwartz, D. A., 1968,
Canadian Journal of Physics 46, S437.
- Riegler, G. R., Boldt, E., and Serlemitsos, P., 1968, Ap. J. 153, L95.
- Sartori, L. and Morrison, P., 1967, Ap. J. 150, 385.
- Seward, F., Chodil, G., Mark, Hans, Swift, C., and Toor, A., 1967, Ap. J. 150,
845.

PRECEDING PAGE BLANK NOT FILMED.

VI. APPENDIX

DATA RETRIEVAL

Because of the large contamination of our record by RF interference, it is necessary to explain, in detail, how the data have been extracted from the record. The electronics system has a 3125 data-word/sec encoder governed by an on-board freely running clock. The details of the format are described by Cancro et al (1968); the only aspect relevant to this discussion is that each of the words describes either (1) a "null event" if there is no acceptable data candidate during the associated 320 μ sec window, or (2) the first acceptable event in the window (it is important to remember that the window start and end times are fixed by a freely running clock, and not by the preceding event).

The RF noise which contaminated our record was a 10 kHz pulse train from a rocket housekeeping transmitter which was detected in the preamplifier of one of the krypton-filled proportional counters. These pulses appeared in the record as data from a single krypton counter, and were, therefore, distinguishable from argon counter events since all detected events were labelled with the identity of the counter in which they were recorded. The nature of the 10 kHz pulse train is such that while the average separation between pulses is 100 μ sec, the minimum separation is 40 μ sec (and the maximum 160 μ sec), so that the counting rate of these pulses is definitely not random.

If a detection system is sampling random events of k types, and the average event rate of the j^{th} type (in k) is r_j , the a priori differential probability of observing a j event in any element of time dt is:

$$p_j dt = r_j dt . \quad (A1)$$

The differential probability that the first event of the j^{th} type will occur during time $t \rightarrow t + dt$ after some arbitrarily specified temporal origin is then:

$$\begin{aligned} p_j^{(1)}(t) dt &= dt \lim_{\Delta t \rightarrow 0} \left[r_j (1 - r_j \Delta t)^{t/\Delta t} \right] \\ &= dt r_j e^{-r_j t}. \end{aligned} \quad (\text{A2})$$

Suppose that the differential probability of observing another type of event q (not necessarily random) in any time dt is $(p_q dt)$. The differential probability of obtaining a j pulse during time $t \rightarrow t + dt$ as the first pulse of any sort (k or q) in the time interval $0 \rightarrow t + dt$ is:

$$p_j^*(t) dt = p_j^{(1)}(t) dt \bar{P}_q(t' < t) \prod_{k \neq j} \bar{P}_k(t' < t). \quad (\text{A3})$$

Where $\bar{P}_m(t' < t)$ is the integral probability that there is no m -type event in the time interval $0 \rightarrow t + dt$.

$$\begin{aligned} \prod_{k \neq j} \bar{P}_k(t' < t) &= \prod_{k \neq j} \left(1 - \int_0^t r_k e^{-r_k t'} dt' \right) \\ &= \prod_{k \neq j} e^{-r_k t}. \end{aligned} \quad (\text{A4})$$

Therefore:

$$p_j^*(t) dt = r_j e^{-Rt} \bar{P}_q(t' < t) dt \quad (\text{A5})$$

where

$$R = \sum_{\text{all } k} r_k . \quad (\text{A6})$$

Since $\bar{P}_q (t' < t)$ is a function of the nature of the q-type events only, it is obvious from Equation (A5) that the relative probability of detecting different types of random events is preserved, even in the presence of non-random events (provided, of course, that there is no correlation between the random and non-random components). If the k types refer to energy bins in the argon and krypton counters, and the q type of event represents the interference, then the shape of the input spectrum deduced from the argon counters cannot be distorted by the interference (note that random noise pulses and background will also have the same relative counting rates with respect to the input spectrum as they would have had if there had been no interference present).

In order to normalize our data we must find the effective percentage live time for the system, which means that we must deduce $\bar{P}_q (t' < t)$. Since there is no correlation between the interference (a nominal 10 kHz clock) and the 3125 Hz encoder clock, the differential probability of having the first q event in the 320 μsec window of an encoder word occurring in the interval $t \rightarrow t + dt$ is

$$\begin{aligned} p_q^{(1)}(t) dt &= f dt && (\text{for } t < f^{-1}) \\ &= 0 && (\text{for } t > f^{-1}) \end{aligned} \quad (\text{A7})$$

where f is the instantaneous frequency of interference pulses.

Equation (A5) then becomes:

$$\begin{aligned}
 p_j^*(t) &= r_j e^{-Rt} (1 - ft) && (\text{for } t < f^{-1}) \\
 &= 0 && (\text{for } t > f^{-1})
 \end{aligned}
 \tag{A8}$$

Since f^{-1} is always less than $320 \mu\text{sec}$, the window for a word, there will always be at least one q event (usually three) in every window, and since the anti-coincidence resolving time is only microseconds, we are virtually certain that the probability for the recording of a null event is vanishingly small (the experimental results bear this out). Therefore, we can assume that each window will contain either a q -type or a k -type event. The probability of recording any k -type event in a $320 \mu\text{sec}$ window is then independent of the width of the window, and equal to:

$$\begin{aligned}
 P_k &= \sum_j^k \int_0^{f^{-1}} p_j^*(t) dt = 1 - \frac{f}{R} (1 - e^{-R/f}) \\
 &= \frac{1}{2} \frac{R}{f} - \frac{1}{6} \left(\frac{R}{f}\right)^2 + \dots
 \end{aligned}
 \tag{A9}$$

Hence, for $R \ll f$ we obtain the approximation

$$P_k \approx \frac{1}{2} \frac{R}{f}
 \tag{A10}$$

However, the instantaneous frequency (f) of interference pulses is not a constant but deviates about 10 kHz by about $\pm 60\%$, maintaining a constant average frequency for sample times of 1.6 msec or greater. Therefore, it is

necessary to define the expectation value for P_k as

$$\langle P_k \rangle_f = \frac{1}{2} R \left\langle \frac{1}{f} \right\rangle_f \quad (A11)$$

The expectation value for the interval between interference pulses is 10^{-4} second, and so the expectation value for P_k over sufficiently long sample times (≥ 1.6 msec) is

$$\langle P_k \rangle_f = \frac{1}{2} (10^{-4}) R. \quad (A12)$$

Although the counting rate goes up by a factor of four when the detector swings from fixed pointing position #1 to fixed pointing position #2, the fraction of recorded to incident photons does not sensibly change since $R/\langle f \rangle$ remains $\ll 1$. The effective percentage live time is:

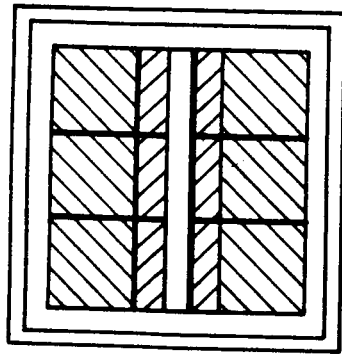
$$\frac{P_k}{R \times 320 \mu\text{sec}} = \frac{1}{2f} \times \frac{1}{320 \mu\text{sec}} = .15625. \quad (A13)$$

The validity of the above expression now depends solely upon how sure we are that $R/f \ll 1$. We can test this hypothesis with the experimental value of P_k (i.e. the fraction of the total recorded events which are k , or random, events) by solving the non-linearized transcendental Equation (A9) for R with $f = \langle f \rangle$. The maximum value of R/f so obtained is .047 so that the effective live time for each of the fixed pointing positions must be that of (A13) to at least three significant figures.

FIGURE CAPTIONS

- 1) The essential elements of the detector. The entrance windows for the argon counters are .002" beryllium; the exit windows of the argon counters and the entrance windows of the krypton counters are .005" beryllium. These gas counters are constructed of beryllium walls; each unit is 6" x 2" x 2". The guard scintillator is viewed by a single 5 inch diameter photomultiplier tube from a position 2 inches below the assembly.
- 2) The apertures for the six fixed targets, as viewed on the celestial sphere. The Crab Nebula is "on axis" for targets #2 and #5, and completely outside the field of view for targets #1 and #6. The angular coordinates, in degrees, are given in declination (δ) and right ascension (RA).
- 3) The total recorded x-ray count for each of the three argon counters (designated I, II, III) is presented for each succeeding dwell position of the rotating plate that modulates the aperture (2.644 seconds per plate position). The total duration of pointing at each of the six fixed targets is indicated along with the corresponding celestial coordinates (RA, δ) of the detector axis. The shaded portions of the record indicate those situations where the beam from Tau XR-1 is completely modulated by the rotating plate.
- 4) The observed spectrum of x-ray counts from Tau XR-1 as recorded by each of the three argon counters, corrected for detection efficiency. The data presented here are from the composite exposure of targets #2 and #5 for counters I and III, and the composite exposure of targets #3 and #4 for counter II.

- 5) The observed spectrum of x-ray counts as recorded by each of the three argon counters, corrected for detection efficiency, during the exposures of targets #1 and #6, for the x-ray background. The unit of time (2.644 sec) corresponds to the dwell time for each position of the rotating plate.



ROTATING COLLIMATOR

GUARD SCINTILLATOR

X-RAY SHIELD

FIXED COLLIMATORS

ARGON PROPORTIONAL COUNTERS (3)

KRYPTON PROPORTIONAL COUNTERS (3)

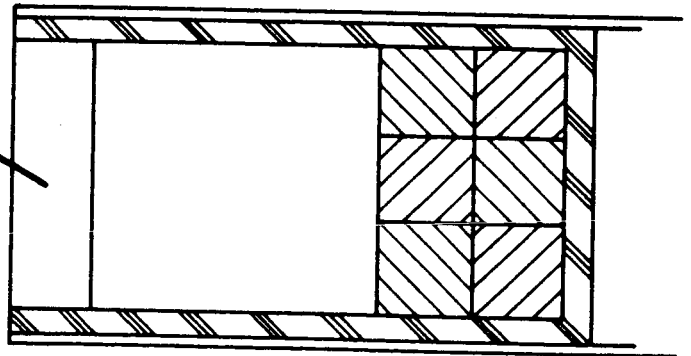
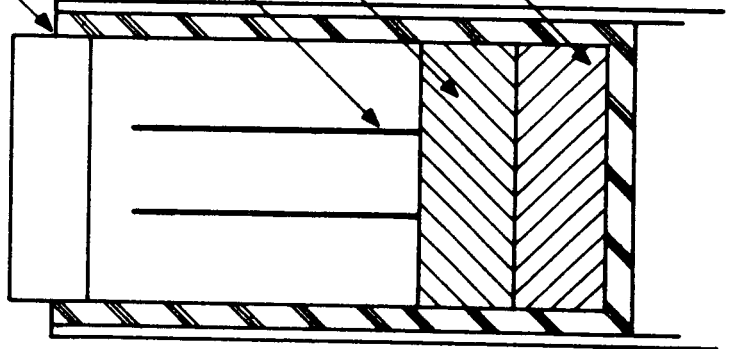
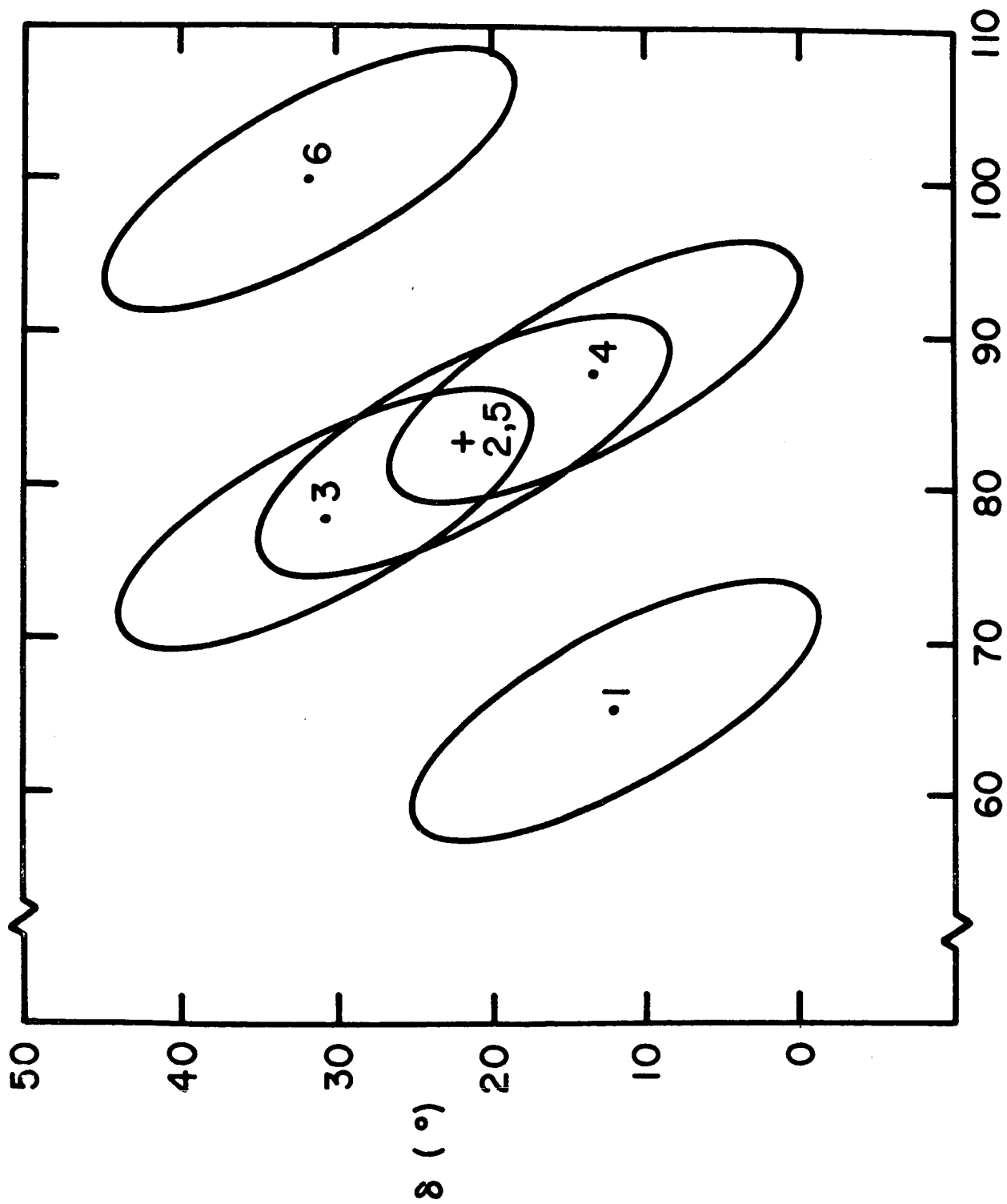


Fig. 1



RA (°)

Fig. 2

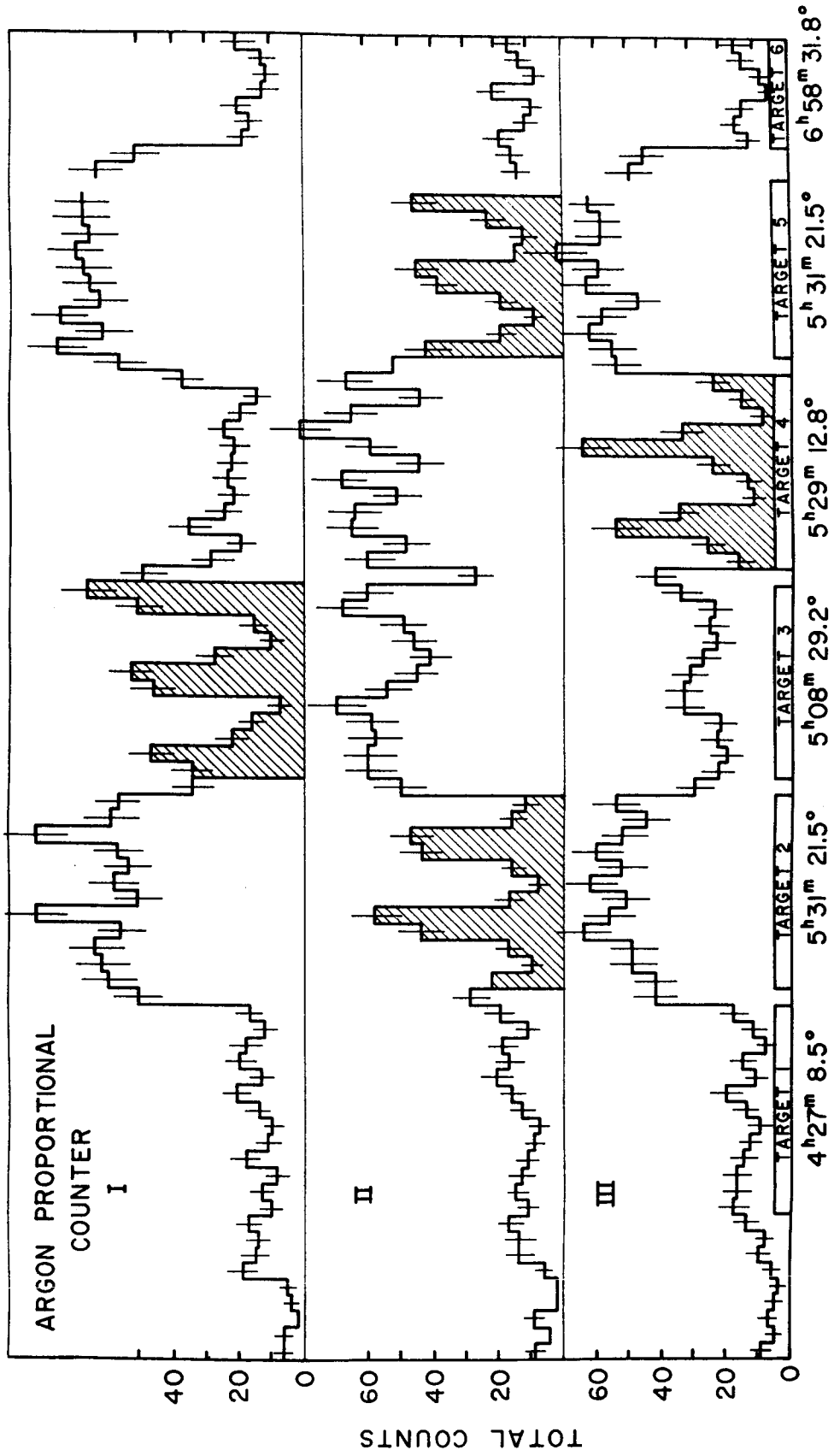
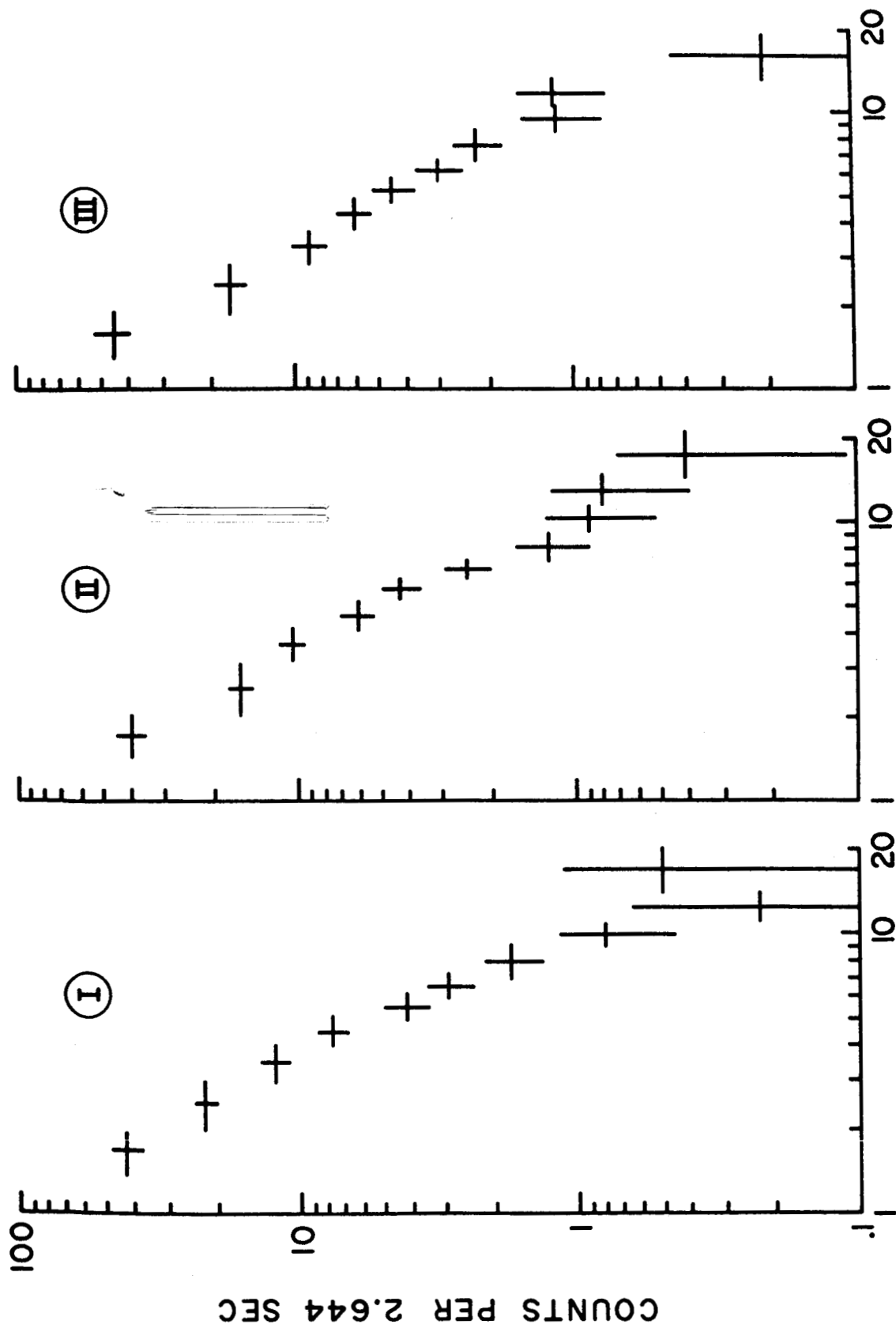
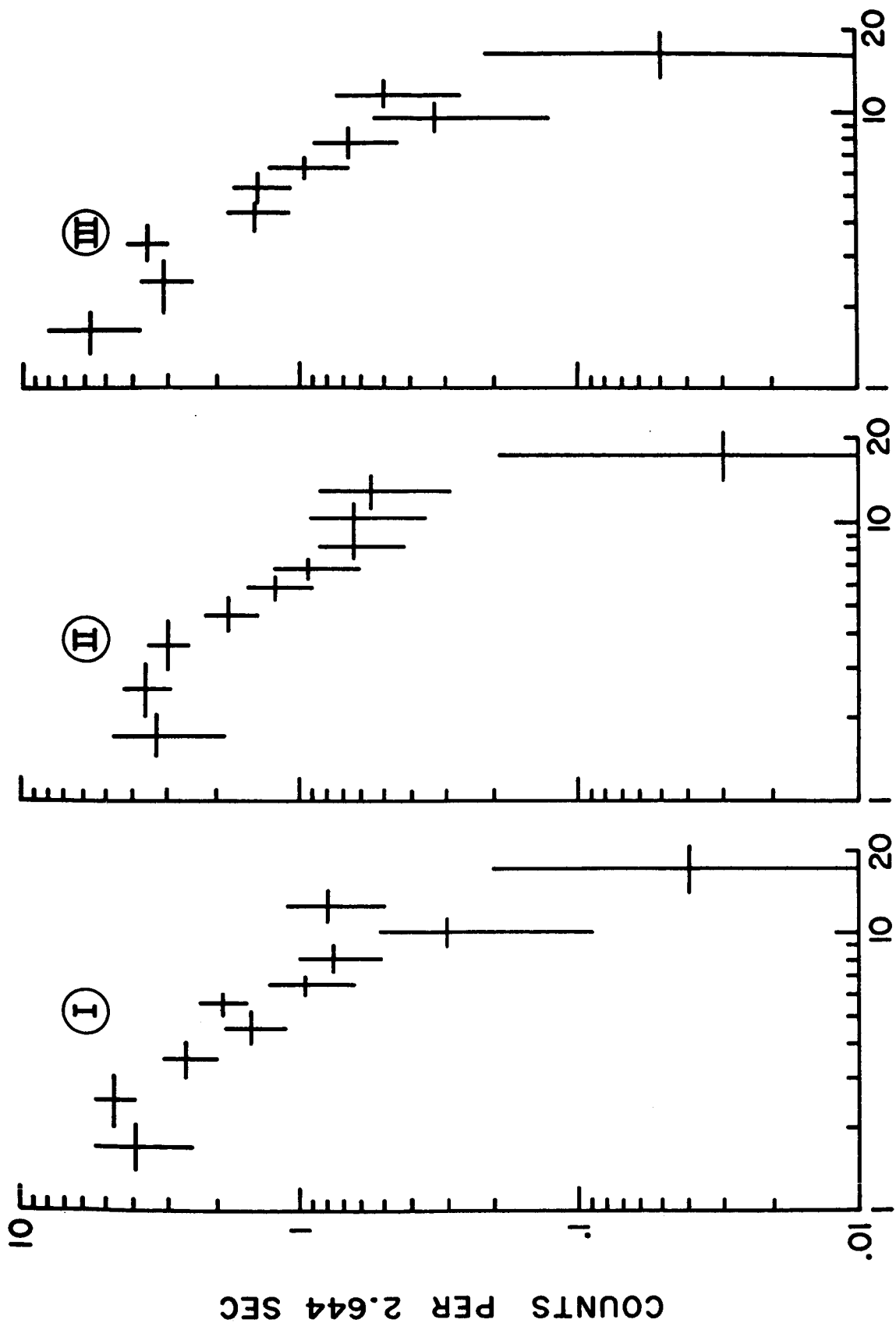


Fig. 3



ENERGY (keV)

Fig. 4



ENERGY (keV)

Fig. 5